MIT Open Access Articles

Renal clearable catalytic gold nanoclusters for in vivo disease monitoring

Renal clearable catalytic gold nanoclusters for *in vivo* disease monitoring

Colleen N. Loynachan[†,1], **Ava P. Soleimany**[†,2,3], **Jaideep S. Dudani**[2,4], **Yiyang Lin**[1], **Adrian Najer**[1], **Ahmet Bekdemir**[2], **Qu Chen**[1], **Sangeeta N. Bhatia**[*,2,5,6,7,8,9], **Molly M. Stevens**[*,1]

[1.] Department of Materials, Department of Bioengineering, and Institute of Biomedical Engineering, Imperial College London, London SW7 2AZ, London, U.K.

[2.] Koch Institute for Integrative Cancer Research, Massachusetts Institute of Technology, Cambridge, MA 02139

[3.] Harvard Graduate Program in Biophysics, Harvard University, Boston, MA 02115

[4.] Department of Biological Engineering, Massachusetts Institute of Technology, Cambridge, MA 02139

[5.] Harvard-MIT Division of Health Sciences and Technology, Institute for Medical Engineering and Science, Massachusetts Institute of Technology, Cambridge, MA 02139

[6.] Department of Electrical Engineering and Computer Science, Massachusetts Institute of Technology, Cambridge, MA 02139

[7.] Department of Medicine, Brigham and Women's Hospital and Harvard Medical School, Boston, MA 02115

[8.] Broad Institute of Massachusetts Institute of Technology and Harvard, Cambridge, MA 02139

9. Howard Hughes Medical Institute, Cambridge, MA 02139

Abstract

Ultra-small gold nanoclusters (AuNCs) have emerged as agile probes for *in vivo* imaging, as they exhibit exceptional tumour accumulation and efficient renal clearance properties. However, their intrinsic catalytic activity, which can enable increased detection sensitivity, has yet to be explored for *in vivo* sensing. By exploiting the peroxidase-mimicking activity of AuNCs and the precise nanometer size filtration of the kidney, we designed multifunctional protease nanosensors that respond to disease microenvironments to produce a direct colorimetric urinary readout of disease state in less than 1 h. We monitored the catalytic activity of AuNCs in collected urine of a mouse model of colorectal cancer where tumour-bearing mice showed a 13-fold increase in colorimetric signal compared to healthy mice. Nanosensors were eliminated completely through hepatic and renal excretion within 4 weeks after injection with no evidence of toxicity. We envision that this modular approach will enable rapid detection of a diverse range of diseases by exploiting their specific enzymatic signatures.

Keywords

MAIN

Democratization of diagnostic tools to enable simple, sensitive, and early detection of disease is essential, particularly in low- and middle-income countries, which bear a significant burden of both infectious and noncommunicable diseases.[1] While worldwide mortality rates due to infectious diseases have substantially decreased, the ever increasing ageing population means cancer has become a primary cause of morbidity and mortality.[2] New globally accessible diagnostic tools will be key in addressing unmet challenges in global oncology. Advances in nanotechnology offer unprecedented solutions in the form of responsive detection tools that, when applied globally, can enable earlier diagnosis and better treatment irrespective of the local resources available.[3]

Early diagnosis of cancer enables effective treatment of primary tumours via local therapeutic interventions such as surgery and radiotherapy.[4] Early detection has largely relied on blood biomarkers. However, the prohibitively low rates that most biomarkers are shed from tumours, the tremendous dilution into circulation, and the lack of specificity of secreted biomarkers impede early detection.[5,6] Protease activities are implicated in a wide range of noncommunicable human diseases including cancer, inflammation, and thrombosis. Monitoring protease activity as a biomarker of disease may be leveraged to overcome the lack of sensitivity and specificity of abundance-based blood biomarkers.[7] Common tools to measure protease activity often rely on cumbersome and infrastructure heavy analyses, such as fluorescence,[8–10] mass spectrometry,[11] or MRI.[12] Previously, we developed exogenously administered multiplexed protease-responsive nanoparticles that release small reporter probes into the urine in response to proteolytic cleavage in disease environments.[3,13–15]

These protease nanosensors offer sensitivity advantages for *in vivo* protease monitoring due to enzymatic amplification and renal concentration of reporter probes from blood to urine, allowing for direct measurement of reporters by mass spectrometry[16] or immunoassays.[13,17] In practice, however, these techniques require analysis and expensive analytical reagents not typically available in resource-limited settings. For precision medicine to become globally accessible, diagnostic tools that can probe protease activity with a simple and sensitive readout are required.

Ultra-small gold nanoclusters (AuNCs, < 2 nm) offer an elegant solution to the need for simple and sensitive diagnostic readouts due to their discrete electronic and molecular-like properties.[18,19] Particularly, noble metal nanoclusters and nanoparticles can function as catalysts to disproportionate or decompose H_2O_2, which in turn can oxidize a chromogenic substrate, providing a colorimetric measure of catalytic activity, similar to the enzyme horseradish peroxidase (HRP).[20–22] Despite this potential to provide a high sensitivity and simple readout for early disease detection, to date AuNCs have been used *in vivo* solely for fluorescence and X-ray contrast bioimaging applications.[23–25] We therefore sought to leverage the catalytic activity of AuNCs to develop a nanosensor platform that produces a direct colorimetric readout of disease state.

Here, we present the design of a versatile and modular nanosensor, comprised of renal clearable catalytic AuNCs tethered via peptide linkages to a larger protein carrier, that is disassembled in response to dysregulated protease activity at the site of disease. To demonstrate the modularity of the system in responding to different families of proteases, we synthesized functionalized peptide substrates shown to be specifically cleaved by either the serine protease thrombin[26,27] or the zinc-dependent matrix metalloproteinase 9 (MMP9), which play a critical role in cardiovascular disease or cancer, respectively.[28,29] We demonstrated the response of our protease nanosensors both *in vitro* and *in vivo*, achieving sensitive disease detection with a rapid, colorimetric urinary readout in a mouse model of colorectal cancer using our MMP-responsive nanosensors. Our system exhibited a dual amplification platform: leveraging both *in vivo* protease activity and inorganic catalytic activity of AuNCs to provide a visual readout of disease state directly in urine. With this method, we demonstrate that these AuNCs are small enough to be filtered efficiently through the kidneys and retain catalytic activity in cleared urine, thus providing a versatile disease detection platform that is compatible for deployment at the point-of-care (PoC).

Peptide-templated catalytic AuNCs with high serum stability

Protease-responsive nanosensors were synthesized using biotinylated protease-cleavable peptides to template and stabilize the growth of catalytic AuNCs, which were further coupled to neutravidin (NAv). Neutravidin was selected as a biocompatible carrier for protease-responsive AuNC reporter probes due to its high affinity for biotin and low nonspecific binding properties (Fig. 1).[30] The AuNC-neutravidin (AuNC-NAv) complex was then intravenously (i.v.) administered and specifically disassembled by proteases at the site of disease. Our system takes advantage of a biological pharmacokinetic switch, where the size of the particle largely drives biodistribution.[31,32] Once proteolytically liberated from the neutravidin complex, AuNCs circulated via the bloodstream and were efficiently filtered into

the urine through the kidneys due to their small size (< 5 nm). A simple colorimetric assay was performed on the urine to assess the presence of AuNCs as an indicator of disease state (Fig. 1).

We used a co-templated approach to synthesize noble metal nanoclusters, incorporating both the tripeptide glutathione (GSH, γ-Glu–Cys–Gly), a common capping ligand in nanocluster synthesis,[23,33] and a thiol-terminated functional protease-cleavable peptide (Table 1) that act as both stabilizing capping ligands and reducing agents for nanoparticle formation (Fig. 2a). Gold was selected as the core metal, as it exhibited the highest catalytic activity compared to platinum and gold-platinum bimetallic hybrid nanoclusters and could be produced with a low coefficient of variation (CoV = 8.5%), an important consideration in designing a scalable diagnostic platform (Supplementary Fig. 1).

The peptide substrates used as templates for AuNC synthesis were composed of three functional domains: an enzyme recognition motif, a C-terminal cysteine residue to provide a thiol group for sequestering Au ions, and an N-terminal biotin ligand for efficient conjugation to a neutravidin carrier protein. The advantage of this synthesis route to produce catalytic noble metal nanoclusters is the ability to incorporate responsive and functional ligands onto the surface through simple gold-thiol interactions in a one-pot synthesis. Additionally, we have previously investigated carrier and linker-specific effects on cleavage rates,[14] and hypothesized that the target protease may be sterically hindered from accessing the scissile bond when the peptide sequence is presented on the AuNC and simultaneously linked to the neutravidin core. To explore this hypothesis, we also synthesized longer peptides (P1$_{20}$, P2$_{20}$) by incorporating glycine spacers between the N-terminus and protease recognition motif (Table 1). We assessed the ability of the relevant protease to cleave the peptide substrate by verifying the mass of fragments after *in vitro* protease degradation (Supplementary Fig. 2).

The AuNCs did not exhibit surface plasmon resonance, a characteristic of large gold nanoparticles, but rather exhibited molecular-like absorption and corresponding fluorescence properties, attributed to the discrete electronic state arising from their size (Supplementary Fig. 3). Transmission electron microscope (TEM) images and size analysis of the peptide-templated AuNCs (Fig. 2b, Supplementary Figs. 4 and 5) showed that the average size (1.5 ± 0.4 nm, Fig. 2c) was below the glomerular filtration cut-off (*ca.* 5.5 nm), making them ideally suited for kidney clearance.[31,32,34–36]

The peroxidase-like catalytic activity of the AuNCs was measured using the oxidation of the peroxidase substrate 3,3′,5,5′-Tetramethylbenzidine (TMB) by H_2O_2 as a model catalytic reaction, and absorbance at 652 nm provided a colorimetric readout of AuNC activity (Fig. 2d, Supplementary Fig. 1 and 6, Supplementary Table 2). To assess the sensitivity of our catalytic reporter probes, we measured the catalytic activity of a dilution series of each AuNC batch in synthetic urine (Fig. 2e) and determined the limit of detection to be *ca.* 2.7 picomoles (25 μL urine, *ca.* 100 nM AuNCs), with a broad linear response and dynamic range spanning over three orders of magnitude of particle concentration.

There are several advantages to using inorganic AuNCs over natural peroxidases. HRP is not feasible to use as a reporter probe in a comparable *in vivo* diagnostic system, as it is not readily cleared through the renal filtration pathway due to its size (*ca.* 4.5 nm) and the tendency for proteins to be reabsorbed by the tubular epithelium.[37] Additionally, HRP would be susceptible to nonspecific degradation by endogenous proteases *in vivo* which would hinder activity of any cleared enzyme.[38] On the other hand, AuNCs showed high stability in physiological environments, maintaining catalytic activity, size, and morphology in the presence of serum, urine, and physiologically relevant glutathione concentrations (Fig. 2f, Supplementary Figs. 7, 8, and 9). A key performance requirement of the AuNCs is that they retain their catalytic activity following exposure to complex environments such as patient serum, which contains *ca.* 7 wt% protein. AuNCs effectively evaded nonspecific protein adsorption, retaining 80 – 90% of catalytic activity after 1 h incubation in fetal bovine serum (undiluted FBS) or synthetic urine compared to PBS controls (Fig. 2f). In deciding which particle platform to take forward *in vivo*, we selected a system that balanced appropriate protease substrate loading with retention of activity (Supplementary Fig. 10).

Renal clearance of AuNCs and activity retention in urine

The high physiological stability and retention of AuNC catalytic activity after exposure to serum and urine offered a unique opportunity to non-invasively monitor AuNC clearance in urine by measuring gold signal using both our catalytic activity assay and inductively coupled plasma-mass spectrometry (ICP-MS) (Fig. 3a). To determine renal clearance efficiency, urine from mice injected with AuNCs was measured against a calibration curve for both catalytic activity and gold content. This showed that up to $73 \pm 7\%$ of the injected dose of functionalized AuNCs left the body via this route at 1 h post injection (p.i.) and retained catalytic activity in urine (Fig. 3b). Encouragingly, the catalytic activity assay and ICP-MS results appeared to correlate (Fig. 3c, Pearson's $r = 0.492$, *$P = 0.0383$). Thus, the catalytic activity assay can provide a simple and sensitive assessment of AuNC presence in urine without the need for ICP-MS. Analysis of urine from mice injected with PBS revealed that no endogenous peroxidase activity was detectable in collected urine (Supplementary Fig. 11). Using TEM image analysis, we confirmed that the size and morphology of AuNCs cleared by the kidneys and excreted into the urine was comparable to as-synthesized AuNCs (Supplementary Fig. 8). This indicates that the particle stability was unperturbed *in vivo*, which is consistent with the retention of the functional properties of the nanoclusters after *in vivo* interrogation.

AuNC nanosensors respond to protease activity *in vitro*

The biotin functional handles on the protease substrate-modified AuNCs were used to tether them to a neutravidin carrier protein to assemble an AuNC-NAv complex. Dynamic light scattering (DLS) was used to monitor the size of the free AuNCs, neutravidin carrier, and assembled AuNC-NAv complex (Supplementary Figs. 12 and 13), with representative hydrodynamic diameters of 2.5 ± 0.6 nm (GSH-AuNC), 3.3 ± 0.7 nm (AuNC-P1$_{20}$), 7.9 ± 1.5 nm (NAv), and 11.3 ± 2.2 nm (AuNC-P1$_{20}$-NAv).

To explore the kinetics of proteolytic cleavage of AuNC-NAv complexes, we employed fluorescence correlation spectroscopy (FCS) as a single-molecule detection method (Fig.

4a). After enzyme incubation, the diffusivity of the complex shifted over time towards that of the free fluorescently labelled clusters, indicating cleavage had occurred (Fig. 4b). Hydrodynamic size analysis by FCS showed that the MMP-responsive AuNC-P2_{20}-NAv complex was completely disassembled within 4.5 h of MMP9 incubation (Fig. 4c). The size of the thrombin-cleavable complex, AuNC-P1_{20}-NAv, did not significantly change when incubated with MMP9, and the size of the MMP-responsive AuNC-P2_{20}-NAv complex did not fall below the renal filtration limit when incubated with an off-target enzyme, in this case thrombin, for 12 h. Taken together, these results show the specificity of our nanosensors for their target enzymes. To demonstrate the modularity of our system, we used FCS to measure the disassembly kinetics of the thrombin-responsive complex (AuNC-P1_{20}-NAv), which was efficiently cleaved by thrombin (Supplementary Fig. 14). Further, MMP9 exhibited a rate of 3% AuNCs cleaved per minute toward the AuNC-P2_{20}-NAv complex, while the rate was only 0.08% AuNCs cleaved per minute toward the AuNC-P2_{13}-NAv complex (Fig. 4d). This *ca.* 40-fold increase in the cleavage rate for the complex formed with the longer linker could be attributed to increased accessibility of the enzyme to the scissile bond. FCS results showed that in the presence of biologically-relevant enzyme concentrations,[39] significant cleavage was observed for AuNC-P2_{20}-NAv complexes, where 80% of AuNCs were cleaved within the first hour of incubation with MMP9.

Proteolytic cleavage of AuNC-NAv complexes was further characterized *in vitro* by incubating complexes with recombinant protease, using gel filtration chromatography (GFC) to separate cleavage products by size, and monitoring cleavage with a catalytic activity assay (Fig. 4e-f and Supplementary Fig. 13). The extent of cleavage of the AuNC-NAv complex under different conditions was quantified by analysing the area under the curve associated with each cleavage product from the activity assay (Supplementary Table 3). Nonspecific cleavage was investigated by incubating AuNC-P1_{20}-NAv with MMP9 and AuNC-P2_{20}-NAv with thrombin. Low background cleavage by the off-target enzyme was observed (Fig. 4e-f), in agreement with FCS results. Finally, we explored the sensitivity of our nanosensor to MMP9 activity *in vitro* using both FCS and a filtration-based colorimetric catalytic activity assay (Supplementary Fig. 15), where low nanomolar sensitivities were observed, comparable to commercial *in vitro* fluorogenic protease activity assays.

Biodistribution and clearance pathways for nanosensors

We assessed the biocompatibility of AuNC-NAv complexes *in vitro* and found that they were non-toxic to HEK293T cells up to 15 μM (Supplementary Fig. 16). Toxicological responses of our AuNC-NAv complexes (3000 pmol AuNC dose) *in vivo* was investigated by examining pathology of the mice after complex injection. No significant changes in bodyweight over 28 days and no histological evidence of heart, lung, liver, spleen, or kidney toxicity were found at both short (1 h) and longer (24 h and 10 days) time points post injection, suggesting that AuNC-NAv complexes did not induce significant systemic toxicity (Supplementary Fig. 16).

To assess clearance time frames and mechanisms, we explored the organ biodistribution, blood pharmacokinetics, urine composition, and elimination pathways of AuNCs and AuNC-NAv complexes labelled with a photostable near-IR dye. From the organ

biodistribution study, free AuNCs accumulated most significantly in the kidneys relative to other organs including the liver at 1 h p.i. and were completely cleared from all major organs within 7 days p.i. To corroborate the biodistribution study, we measured gold signal in the urine by ICP-MS and our catalytic activity assay, where the presence of AuNCs was undetectable after 24 h p.i. (Supplementary Fig. 17, Supplementary Table 4). Due to their size (*ca.* 11 nm), the intact AuNC-NAv complexes accumulated predominately in reticuloendothelial system (RES) organs.[40] The AuNC-NAv signal in the liver increased up to 24 h p.i., significantly decreased after 1 week, and was completely undetectable in all major organs 4 weeks p.i. (Supplementary Fig. 18). Encouragingly, the biodistribution and histology results suggest that, in healthy animals, intact AuNC-NAv complexes were cleared from the circulation and taken up in RES organs and eliminated completely through hepatic (bile to faeces) and renal (urine) excretion within 4 weeks p.i. with no evidence of systemic or tissue-level toxicity.

AuNC nanosensors enable colorimetric urinary disease detection

After confirming successful cleavage by recombinant proteases *in vitro*, we sought to apply the protease-responsive AuNC nanosensor platform to *in vivo* disease detection using the colorimetric urinary readout. We characterized the pharmacokinetics of the neutravidin carrier, AuNC-NAv complex, and free AuNCs in terms of accumulation in organs and tumour xenografts of the human colorectal cancer cell line LS174T, which secretes MMP9[13] (Supplementary Fig. 19). Based on the measured blood half-life of the AuNC-NAv complex and the degree of tumour accumulation within 1 h p.i., we selected 1 h after nanosensor injection as our time point for urine collection.

For *in vivo* tumour detection experiments, tumour-bearing and healthy control mice were intravenously injected with MMP-responsive AuNC-P2$_{20}$-NAv nanosensors (Fig. 5a). Urine was collected from mice 1 h p.i., and the catalytic activity assay was run using 25 μL of urine sample. Comparing signal from healthy and tumour-bearing mice, we observed a blue colour that could be read by eye in urine samples from tumour-bearing mice after the addition of the chromogenic peroxidase substrate, TMB (Fig. 5b). Quantification revealed a mean urinary signal increase of approximately 13-fold in tumour-bearing mice relative to healthy mice, as measured by the direct colorimetric readout and initial velocity analysis (A$_{652}$ min^{-1}) of cleared AuNC catalytic activity in collected urine (Fig. 5c). The AuNC catalytic activity measured corresponded to *ca.* 3.2% of the injected dose in urine from tumour-bearing mice compared to 0.2% renal clearance in healthy mice, normalized using urine volumes (Supplementary Fig. 20). We believe our platform might benefit from improved diffusion, transport, tumour accumulation, and clearance properties of peptide-templated gold nanoclusters compared to larger nanomaterials commonly used in delivery applications, where only *ca.* 0.7% of the administered nanoparticle dose was reported to be delivered to the solid tumour.[41–43] Receiver operating characteristic (ROC) analysis revealed that the colorimetric test was highly accurate and discriminated the presence of colorectal cancer xenografts with an area under the curve (AUC) of 0.91 (Fig. 5d, *P* = 0.0002). Furthermore, the delivery of our nanosensors to malignant tissues can be enhanced by exploiting our one-pot synthesis scheme for the incorporation of active targeting ligands, *e.g.*, the integrin-targeting ligand iRGD,[14] onto the surface of the AuNCs.

Having established that the MMP-responsive AuNC nanosensors could discriminate between tumour-bearing and healthy mice, we sought to assess whether the urinary signal was driven by disease-associated protease activity. There was no significant difference in urine volumes between the groups, and analysis of urine samples from PBS-injected healthy and tumour-bearing mice confirmed that no endogenous peroxidase activity was present in the absence of injected nanosensors (Supplementary Fig. 20). TEM image analysis of urine from tumour-bearing mice confirmed the presence of AuNCs cleared by the kidney, with size and morphology comparable to as-synthesized AuNCs (Supplementary Fig. 8c). To ensure that the AuNC-NAv complex was not disassembling *in vivo* due to poor chemical stability or nonspecific cleavage, we tested a substrate that we did not expect to be specifically cleaved in the tumour model.[17] Thrombin-responsive AuNC-P1$_{20}$-NAv complexes were injected into tumour-bearing and healthy mice and did not result in any significant colorimetric signal in urine from tumour-bearing mice compared to healthy controls (Fig. 5e). This pattern suggested that there is a non-promiscuous release of AuNCs *in vivo* from AuNC-P2$_{20}$-NAv complexes that is amplified in tumour-bearing mice, where elevated MMP levels at the site of disease and in circulation may actively disassemble AuNC-NAv complexes. Taken together, these results demonstrate that the AuNC-NAv nanosensors respond to disease-specific proteolytic activity *in vivo* and enable a direct colorimetric readout of disease state, as evidenced by highly accurate discrimination in a flank tumour model of human colorectal cancer.

CONCLUSIONS

We have developed a modular approach for rapid detection of a disease state based on a simple and sensitive colorimetric urinary assay that requires minimal equipment and can be read by eye in < 1 h. We synthesized *ca.* 2 nm catalytic gold nanocluster probes modified with orthogonal protease substrates, which are responsive to multiple enzymes. We demonstrated that the peptide-templated AuNCs can be filtered through the kidneys and excreted into the urine with high efficiency and retain catalytic activity in complex physiological environments. We assembled the AuNC probes into larger complexes, which were disassembled in response to specific proteases. Finally, we deployed MMP-responsive AuNC-NAv complexes *in vivo* in a colorectal cancer mouse model and successfully detected AuNCs in urine from tumour-bearing mice with a facile colorimetric readout.

Here, we have shown that through rational surface modification of AuNCs, we can engineer nanosensors that can be deployed *in vivo* and exploit intrinsic catalytic activity of renal clearable noble metal nanoclusters as a disease indicator. We present a versatile toolbox that can be used to probe the complex enzymatic profiles of specific disease microenvironments, the results of which will open new opportunities for developing translatable responsive and catalytic nanomaterial diagnostics for a range of diseases in which enzyme activity can be used as a biomarker. We envision that clinical application of this technology may additionally take advantage of multiplexed protease substrate linkages, such as those responsive to Boolean logic operations,[44,45] which may be able to profile the activities of proteases of diverse classes in order to distinguish between cancers and other pathologies. Our adaptable nanocatalyst amplification platform should be applicable in low-resource settings for rapid detection of a diverse range of disease-associated proteases, including

those implicated in infectious diseases, and will democratize access to advanced and sensitive diagnostics.

METHODS

Materials

All chemicals were purchased from Sigma-Aldrich unless otherwise stated. Milli-Q water (18.2 MΩ.cm) was used in all the experiments.

AuNC synthesis

Synthesis and purification of peptide-capped AuNCs followed published procedures with modifications outlined below.[1] We varied the ratio of protease-cleavable peptide substrate to glutathione in the AuNC synthesis to incorporate functional handles onto the AuNC surface (P1:GSH or P2:GSH, tested at 1:2, 1:4, 1:5, 1:9). Briefly, freshly prepared aqueous solution of gold(III) chloride trihydrate (HAuCl$_4$, 20 mM, 100 μL) was mixed with 750 μL deionized water in an Eppendorf tube, followed by fast addition of L-Glutathione reduced (GSH, 20 mM) and either peptide P1 or P2 (20 mM) so that final peptide content was fixed at a total volume of 150 μL in varying ratios of P1 or P2:GSH at 25 °C. The reaction mixture was heated to 70 °C under gentle stirring (500 rpm) for 24 h. The reaction mixture changed from yellow to colourless within minutes and then turned pale yellow over *ca.* 12 h, indicating first reduction of Au (III) to Au (I) by the thiol group of the peptides, followed by the reduction of Au(I) thiolate complexes to Au(0) atoms over time assisted by the favourable reduction kinetics at the elevated reaction temperature.[2,3] After 24 h synthesis, the resulting AuNC solution exhibited both orange luminescence and simultaneous peroxidase-like activity. The AuNCs could be stored at 4 °C for > 6 months with negligible changes in optical or catalytic properties. The as-prepared AuNCs were purified through centrifugal ultrafiltration (Amicon Ultra centrifugal filter units Ultra-15, MWCO 10 kDa, Sigma) and buffer exchanged into phosphate buffered saline (PBS, pH 7.2). During ultrafiltration, the AuNCs were collected in the concentrate in the filter device, while any unbound peptide was collected in the filtrate. After purification, AuNCs were resuspended in PBS (20 μM by AuNC particle concentration) and sterile filtered (Millex-GV Filter, Millipore, 0.22 μm).

The number of biotinylated ligands per AuNC was calculated by measuring biotin concentration in the filtrate from AuNC purification above, and subsequently subtracting this value from the starting concentration of biotinylated peptide used in the synthesis. Biotin concentration in the filtrate was quantified using the Pierce Biotin Quantitation kit in a 96-well plate following manufacturer's instructions (Thermo Fisher) without any modifications. The molarity of biotin in the sample was calculated using the extinction coefficient for HABA/avidin at 500 nm of 34,000 M^{-1}cm^{-1} and path length of 0.5 cm.

Characterization of nanoparticles

Dynamic light scattering (DLS, Zeta Sizer Nanoseries, Malvern Instruments, Ltd.) was used to characterize the hydrodynamic diameter of nanoparticles. Absorption measurements were recorded on a SpectraMax M5 multimode microplate reader (Molecular Devices, Ltd.) using SoftMax Pro (Version 5.4) software. For electron microscopy characterization, samples were

drop-casted onto carbon-coated copper grids (Electron Microscopy Sciences), and TEM imaging was performed using a JEOL 2100F operating at 200 kV. For preparation of TEM samples, AuNC samples were first desalted (Zeba Spin Desalting Columns, 7K MWCO, Sigma) and 5 μL desalted sample was dropped onto the grid, allowed to incubate for 5 min, and subsequently wicked with filter paper and dried overnight before imaging.

Evaluation of peroxidase-like activity

The colorimetric readout was carefully optimized to maximize signal intensity from AuNCs by varying the concentration of hydrogen peroxide, pH, and concentration of sodium chloride, and measuring corresponding catalytic activity under these conditions (Supplementary Fig. 6, Supplementary Table 2). For stability and catalytic activity of AuNCs in physiological environments, AuNCs (20 μM, 50 μL) were incubated with PBS (50 μL), synthetic urine (Surine Negative Urine Control, Sigma), or fetal bovine serum (FBS, Gibco) for 1 h at 37 °C followed by five-fold dilution in water. For the activity assay, 50 uL of each sample was added to a 96-well plate (Corning, UK) followed by 150 uL chromogenic substrate solution: 1-Step Ultra TMB ELISA Substrate Solution (Thermo Fisher) spiked to a final concentration of 4 M hydrogen peroxide (30% (w/w), Sigma). The absorbance of the reaction solution at 652 nm was monitored up to 25 min after addition of substrate, corresponding to oxidation of TMB by H_2O_2.

For limit of detection (LoD) assays, in a 96-well plate, synthetic urine (25 μL) was mixed with AuNCs (25 μL, varying concentrations, diluted in PBS), 5 M H_2O_2 (100 μL), and 1-Step Ultra TMB ELISA Substrate Solution (100 μL). Absorbance at 652 nm was measured every 20 s for 10 min, and linear regression was used to calculate the slope ($A_{652\ nm}\ s^{-1}$) over the first 150 sec. LoD was calculated as 3 standard deviations above the mean background signal.

AuNC-NAv complex assembly

In a typical conjugation, 125 μL NeutrAvidin Protein (120 μM, PBS, Thermo Fisher, NAv) was mixed with 1 mL of AuNC-P1 or AuNC-P2 (20 μM) and incubated for 12 h gently shaking (500 rpm) at 37 °C. Unbound AuNCs were removed from AuNC-NAv complexes through centrifugal ultrafiltration (Amicon Ultra centrifugal filter units Ultra-15, MWCO 50 kDa, Sigma), where AuNC-NAv complexes remained in concentrate and any unbound AuNCs were collected in the filtrate. After ultrafiltration, AuNC-NAv complexes were resuspended in PBS (30 μM by [AuNC]) and sterile filtered (Millex-GV Filter, Millipore, 0.22 μm).

In vivo renal clearance studies

All animal studies were approved by the Massachusetts Institute of Technology (MIT) committee on animal care (MIT protocol 0417–025-20). All animals received humane care, and all experiments were conducted in compliance with institutional and national guidelines. GSH-templated and substrate functionalized AuNCs were diluted to 10 μM [AuNC] in sterile PBS. Female Swiss Webster mice (4–6 weeks old, Taconic) were intravenously administered 2000 pmol AuNCs via the tail vein (10 μM [AuNC], 200 μL). The injected dose of glutathione-templated gold nanoclusters ranged from 1.6 to 2.4 mg kg^{-1} in terms of

gold content, which is well below the maximal tolerated dose reported for both mice and non-human primates (1059 mg kg^{-1} by GSH-AuNC content, ~530 mg kg^{-1} by gold content).[4]

After nanocluster injection, urine was collected at the indicated timepoints for catalytic activity assay and ICP-MS measurements. Mice were placed in custom housing with a 96-well plate base for urine collection. After 1 h, their bladders were voided, and collected urine volume was measured. Clearance of active AuNCs was quantified via catalytic activity assay, and urine gold content was quantified by ICP-MS. Catalytic activity and gold content measurements of the collected urine samples were compared to that of the injected dose and normalized using urine volumes. Urine concentration may be dependent on many host and environmental factors, and therefore normalization between urine samples is required. In this study we used urine volume and injected dose for normalization. Alternatively, co-administered free reporters that pass into urine independent of disease state, such as glutamate fibrinopeptide B[5] or inulin,[6] could also be measured in urine and used to normalize the level of AuNCs released by protease activity. Pearson's correlation coefficient (r) was computed to assess the relationship between renal clearance as measured by catalytic activity assay or ICP-MS (gold content).

Urine catalytic activity assays

For all assays, 25 μL of urine was diluted into 25 μL PBS in a transparent 96-well plate and allowed to equilibrate at room temperature for 15 min. 100 μL each of 5 M H_2O_2 (Sigma) and TMB (Thermo Fisher) were then added, and the plate was read kinetically at 652 nm over the course of 30 min. In all catalytic activity assays involving AuNCs in collected urine, the final pH was acidic due to the acidic pH of the TMB and hydrogen peroxide substrate mix resulting in a final reaction pH < 4. For renal clearance studies, the concentration of active AuNCs present in the urine was quantified via reference to a calibration curve of known AuNC concentrations. For disease detection studies, the initial reaction velocity was quantified as the rate of change of the absorbance at 652 nm over the first 10 min of the reaction (A_{652} min^{-1}). Initial velocity analysis was preferred over analysis of a single time point measurement of absorbance at 652 nm, as urine collected from different mice had varying degrees of background levels of absorbance at this wavelength based on the hydration state of each mouse. This variable background was removed in the initial velocity analysis as the background absorbance from initial coloration of urine was constant over time. Limit of detection was calculated to be the lowest concentration of the linear portion of the calibration curve (measured as the initial velocity of catalytic activity of relevant AuNC batch).

Inductively coupled plasma-mass spectrometry (ICP-MS) on urine samples

Urine samples were digested in aqua regia (TraceMetal Grade hydrochloric acid, Fisher Chemical; ARISTAR ULTRA nitric acid, VWR) for 24 h. The digested samples were further diluted into an ICP-MS matrix composed of 4% HCl / 4% HNO_3. The gold content in each sample was measured using an Agilent 7900 ICP-MS using an indium internal standard (5 ppb; TraceCERT, Sigma) and gold standard (Inorganic Ventures) for the calibration curve prepared in the ICP-MS matrix.

Cell culture

For xenograft studies, LS174T (ATCC CL-188) cells were cultured in Eagle's Minimal Essential Medium (EMEM, ATCC) supplemented with 10% (v/v) FBS (Gibco) and 1% (v/v) penicillin-streptomycin (CellGro). For *in vitro* cytotoxicity assays, HEK293T (ATCC CRL-3216) cells were cultured in Dulbecco's Modified Eagle Medium (DMEM, ATCC) supplemented with 10% (v/v) FBS (Gibco) and 1% (v/v) penicillin-streptomycin (CellGro). Cells were passaged when confluence reached 80%.

In vitro cytotoxicity studies

For *in vitro* cytotoxicity studies, HEK293T cells were plated in a 96-well plate (10,000 cells per well) and allowed to adhere to the wells. 24 h post seeding, cells were incubated with varying concentrations of AuNC-NAv complex (diluted in PBS) for 24 h. Cell viability was evaluated using the MTS (3-(4,5-dimethylthiazol-2-yl)-5-(3-carboxymethoxyphenyl)-2-(4-sulfophenyl)-2H-tetrazolium) assay (Promega).

In vivo toxicity studies

AuNC-NAv complex (AuNC-P1$_{20}$-NAv or AuNC-P2$_{20}$-NAv, 15 μM [AuNC], 200 μL ~ 3000 pmol) was intravenously injected into immunocompetent female Swiss Webster mice (4–6 weeks old, Taconic). The mass of each mouse was monitored for 4 weeks p.i. and compared with masses of PBS injected control mice. Heart, lung, liver, spleen, and kidney tissues were collected from the mice at 1 h, 24 h, or 10 days p.i., fixed in 10 wt% formalin, paraffin embedded, stained with haematoxylin and eosin, and then examined by a veterinary pathologist and compared to organs from PBS injected control mice.

Pharmacokinetic studies

To analyse the blood half-life of the AuNC-NAv complex, female Swiss Webster mice (4–6 weeks old, Taconic) were injected with AuNC-P2$_{20}$-NAv (15 μM [AuNC], 200 μL ~ 3000 pmol) labelled with the photostable near-IR dye Alexa Fluor 750 Succinimidyl Ester (Invitrogen). Blood was withdrawn retro-orbitally (~70 μL) and then immediately transferred into 70 μL of PBS with 5 mM EDTA and centrifuged to pellet blood cells. Concentration of the AuNC-NAv complex in plasma was measured using an Odyssey CLx infrared scanner (Li-Cor Inc.).

For biodistribution studies in healthy animals, female Swiss Webster mice (4–6 weeks old, Taconic) were injected with either near-IR dye labelled AuNCs (10 μM [AuNC], 200 μL ~ 2000 pmol) or AuNC-P2$_{20}$-NAv (15 μM [AuNC], 200 μL ~ 3000 pmol) complexes. Mice were sacrificed at 1 h, 3 h, 24 h, 1 week, or 4 weeks p.i., and organ and tumour accumulation was measured using an Odyssey CLx scanner (Li-Cor Inc.) and quantified using ImageStudio (Version 5.2, Li-Cor Inc.). Organ accumulation was quantified as signal intensity per unit area, calculated for each organ as the difference between the experimental group (near-IR dye labelled AuNCs or AuNC-P2$_{20}$-NAv) versus the PBS-injected control. Values were scaled by a constant factor for all time points within each treatment group (near-IR dye labelled AuNCs or AuNC-P2$_{20}$-NAv) to fall within the range shown. For mice injected with free AuNCs, urine was also collected at the indicated time points and analysed by both ICP-MS (for gold content analysis) and catalytic activity assay.

For biodistribution studies in tumour-bearing mice, nude mice bearing LS174T flank tumours were infused with either near-IR dye labelled neutravidin carrier (VivoTag750, PerkinElmer; 1 μM by VT750), MMP-cleavable AuNC-P2$_{20}$-NAv complex (15 μM [AuNC], 200 μL ~ 3000 pmol, Alexa Fluor 750), or free AuNCs (10 μM [AuNC], 200 μL ~ 2000 pmol, Alexa Fluor 750). Mice were sacrificed 1 h p.i., and organ and tumour accumulation were measured using an Odyssey CLx scanner (Li-Cor Inc.) and quantified using ImageStudio (Version 5.2, Li-Cor Inc.). Organ accumulation was quantified as signal intensity per unit area, calculated for each organ as the difference between the experimental group (fluorescently labelled carrier, complex, or free nanocluster) versus the PBS-injected control, and scaled to fall within the range shown.

Colorectal cancer xenograft studies

Female NCr Nude mice (4–5 weeks, Taconic) were injected bilaterally with 3×10^6 LS174T cells per flank. Two weeks after inoculation, tumour-bearing mice and age-matched controls were injected with either 15 μM MMP-sensitive or thrombin-sensitive (control) AuNC nanosensors in 200 μL of PBS (concentrations determined by [AuNC]). After nanosensor injection, mice were placed in custom housing with a 96-well plate base for urine collection. Based on the measured blood half-life of the AuNC-NAv complex, the degree of tumour accumulation 1 h p.i., as well as our results from the FCS cleavage assays (80% of AuNCs cleaved from complex within 1 h), we selected 1 h p.i. as our time point for urine collection. [5,7,8] After 1 h, bladders of the mice were voided to collect between 100–200 μL of urine. Urine was analysed via the catalytic activity measurements described above.

Statistical analyses

All statistical analyses were conducted in GraphPad 7.0 (Prism). All sample sizes and statistical tests are specified in figure legends. The D'Agostino-Pearson test was used to assess normality and thus determined the statistical test used. For each animal experiment, groups were established before tumorigenesis or treatment with AuNC-PX, and therefore no randomization was used in the allocation of groups. Investigators were not blinded to the groups and treatments during the experiments.

Supplementary Material

Refer to Web version on PubMed Central for supplementary material.

Acknowledgements

Abbreviations

|	
AuNC	gold nanocluster
GSH	glutathione
i.v.	intravenous
MMP	matrix metalloproteinase
NAv	neutravidin protein
p.i	post injection
PoC	point-of-care
TMB, 3,3′,5,5′	Tetramethylbenzidine
THR	thrombin

REFERENCES

1. World Health Organization. Global action plan for the prevention and control of noncommunicable diseases 2013-2020. (2013).

2. Selmouni F et al. Tackling cancer burden in low-income and middle-income countries: Morocco as an exemplar. Lancet Oncol. 19, e93–e101 (2018). [PubMed: 29413484]

3. Kwon EJ, Lo JH & Bhatia SN Smart nanosystems: Bio-inspired technologies that interact with the host environment. Proc. Natl. Acad. Sci 112, 14460–14466 (2015). [PubMed: 26598694]

4. Etzioni R et al. The case for early detection. Nat. Rev. Cancer 3, 235 (2003).

5. Hori SS & Gambhir SS Mathematical Model Identifies Blood Biomarker-Based Early Cancer Detection Strategies and Limitations. Sci. Transl. Med 3, 109ra116 (2011).

6. Henry NL & Hayes DF Cancer biomarkers. Mol. Oncol 6, 140–146 (2012). [PubMed: 22356776]

7. Lopez-Otin C & Bond JS Proteases: Multifunctional Enzymes in Life and Disease. J. Biol. Chem 283, 30433–30437 (2008). [PubMed: 18650443]

8. Hilderbrand SA & Weissleder R Near-infrared fluorescence: application to in vivo molecular imaging. Curr. Opin. Chem. Biol 14, 71–79 (2010). [PubMed: 19879798]

9. Whitney M et al. Ratiometric activatable cell-penetrating peptides provide rapid in vivo readout of thrombin activation. Angew. Chemie - Int. Ed 52, 325–330 (2013).

10. Whitley MJ et al. A mouse-human phase 1 co-clinical trial of a protease-activated fluorescent probe for imaging cancer. Sci. Transl. Med 8, (2016).

11. Yepes D et al. Multiplex profiling of tumor-associated proteolytic activity in serum of colorectal cancer patients. Proteomics - Clin. Appl 8, 308–316 (2014).

12. Choi JS et al. Distance-dependent magnetic resonance tuning as a versatile MRI sensing platform for biological targets. Nat. Mater 16, 537–542 (2017). [PubMed: 28166216]

13. Warren AD, Kwong GA, Wood DK, Lin KY & Bhatia SN Point-of-care diagnostics for noncommunicable diseases using synthetic urinary biomarkers and paper microfluidics. Proc. Natl. Acad. Sci. U. S. A 111, 3671–6 (2014). [PubMed: 24567404]

14. Kwon EJ, Dudani JS & Bhatia SN Ultrasensitive tumour-penetrating nanosensors of protease activity. Nat. Biomed. Eng 1, 0054 (2017). [PubMed: 28970963]

15. Schuerle S, Dudani JS, Christiansen MG, Anikeeva P & Bhatia SN Magnetically Actuated Protease Sensors for in Vivo Tumor Profiling. Nano Lett. 16, 6303–6310 (2016). [PubMed: 27622711]

16. Kwong GA et al. Mass-encoded synthetic biomarkers for multiplexed urinary monitoring of disease. Nat. Biotechnol 31, 63–70 (2013). [PubMed: 23242163]

17. Dudani JS, Buss CG, Akana RTK, Kwong GA & Bhatia SN Sustained-Release Synthetic Biomarkers for Monitoring Thrombosis and Inflammation Using Point-of-Care Compatible Readouts. Adv. Funct. Mater 26, 2919–2928 (2016). [PubMed: 29706854]

18. Jin R Quantum sized, thiolate-protected gold nanoclusters. Nanoscale 2, 343–362 (2010).

19. Jin R, Zeng C, Zhou M & Chen Y Atomically Precise Colloidal Metal Nanoclusters and Nanoparticles: Fundamentals and Opportunities. Chem. Rev 116, 10346–10413 (2016). [PubMed: 27585252]

20. Xia X et al. Pd-Ir Core-Shell Nanocubes: A Type of Highly Efficient and Versatile Peroxidase Mimic. ACS Nano 9, 9994–10004 (2015).

21. Loynachan CN et al. Platinum Nanocatalyst Amplification: Redefining the Gold Standard for Lateral Flow Immunoassays with Ultrabroad Dynamic Range. ACS Nano 12, 279–288 (2018).

22. Tao Y, Li M, Ren J & Qu X Metal nanoclusters: novel probes for diagnostic and therapeutic applications. Chem. Soc. Rev 44, 8636–8663 (2015). [PubMed: 26400655]

23. Zhang X-D et al. Ultrasmall glutathione-protected gold nanoclusters as next generation radiotherapy sensitizers with high tumor uptake and high renal clearance. Sci. Rep 5, 8669 (2015). [PubMed: 25727895]

24. Chen Y et al. Shortwave Infrared in Vivo Imaging with Gold Nanoclusters. Nano Lett. 17, 6330–6334 (2017). [PubMed: 28952734]

25. Yang W, Guo W, Chang J & Zhang B Protein/peptide-templated biomimetic synthesis of inorganic nanoparticles for biomedical applications. J. Mater. Chem B 5, 401–417 (2017).

26. Davie EW & Kulman JD An Overview of the Structure and Function of Thrombin. Semin. Thromb. Hemost 32, 3–15 (2006).

27. ten Cate H & Hemker HC Thrombin Generation and Atherothrombosis: What Does the Evidence Indicate? J. Am. Heart Assoc 5, 1–8 (2016).

28. Roy R, Yang J & Moses MA Matrix metalloproteinases as novel biomarkers and potential therapeutic targets in human cancer. J. Clin. Oncol 27, 5287–5297 (2009). [PubMed: 19738110]

29. Dudani JS, Warren AD & Bhatia SN Harnessing Protease Activity to Improve Cancer Care. Annu. Rev. Cancer Biol 2, 53–76 (2018).

30. Jain A, Barve A, Zhao Z, Jin W & Cheng K Comparison of Avidin, Neutravidin, and Streptavidin as Nanocarriers for Efficient siRNA Delivery. Mol. Pharm 14, 1517–1527 (2017). [PubMed: 28026957]

31. Soo Choi H et al. Renal clearance of quantum dots. Nat. Biotechnol 25, 1165–1170 (2007). [PubMed: 17891134]

32. Du B, Yu M & Zheng J Transport and interactions of nanoparticles in the kidneys. Nat. Rev. Mater 3, 358–374 (2018).

33. Luo Z et al. From aggregation-induced emission of Au(I)-thiolate complexes to ultrabright Au(0)@Au(I)-thiolate core-shell nanoclusters. J. Am. Chem. Soc 134, 16662–16670 (2012). [PubMed: 22998450]

34. Yu M et al. Noninvasive Staging of Kidney Dysfunction Enabled by Renal-Clearable Luminescent Gold Nanoparticles. Angew. Chemie - Int. Ed 55, 2787–2791 (2016).

35. Ning X et al. Physiological stability and renal clearance of ultrasmall zwitterionic gold nanoparticles: Ligand length matters. APL Mater. 5, (2017).

36. Liu J et al. Passive tumor targeting of renal-clearable luminescent gold nanoparticles: Long tumor retention and fast normal tissue clearance. J. Am. Chem. Soc 135, 4978–4981 (2013). [PubMed: 23506476]

37. Straus W Renal reabsorption and excretion of horseradish peroxidase. Kidney Int. 16, 404–408 (1979). [PubMed: 393894]

38. Manning MC, Chou DK, Murphy BM, Payne RW & Katayama DS Stability of protein pharmaceuticals: An update. Pharm. Res 27, 544–575 (2010). [PubMed: 20143256]

39. Kwong GA et al. Mathematical framework for activity-based cancer biomarkers. Proc. Natl. Acad. Sci 112, 12627–12632 (2015). [PubMed: 26417077]

40. Yu M & Zheng J Clearance Pathways and Tumor Targeting of Imaging Nanoparticles. ACS Nano 9, 6655–6674 (2015).

41. Dai Q et al. Quantifying the Ligand-Coated Nanoparticle Delivery to Cancer Cells in Solid Tumors. ACS Nano 12, 8423–8435 (2018). [PubMed: 30016073]

42. Tang S et al. Tailoring Renal Clearance and Tumor Targeting of Ultrasmall Metal Nanoparticles with Particle Density. Angew. Chemie - Int. Ed 55, 16039–16043 (2016).

43. Wilhelm S et al. Analysis of nanoparticle delivery to tumours. Nat. Rev. Mater 1, 16014 (2016).

44. Von Maltzahn G et al. Nanoparticle self-assembly gated by logical proteolytic triggers. J. Am. Chem. Soc 129, 6064–6065 (2007). [PubMed: 17447766]

45. Badeau BA, Comerford MP, Arakawa CK, Shadish JA & Deforest CA Engineered modular biomaterial logic gates for environmentally triggered therapeutic delivery. Nat. Chem 10, 251–258 (2018). [PubMed: 29461528]

References (Methods section)

1. Zhang X-D et al. Ultrasmall glutathione-protected gold nanoclusters as next generation radiotherapy sensitizers with high tumor uptake and high renal clearance. Sci. Rep 5, 8669 (2015). [PubMed: 25727895]

2. Yu Y, Luo Z, Yu Y, Lee JY & Xie J Observation of cluster size growth in CO-directed synthesis of Au 25(SR) 18 nanoclusters. ACS Nano 6, 7920–7927 (2012).

3. Luo Z et al. From aggregation-induced emission of Au(I)-thiolate complexes to ultrabright Au(0)@Au(I)-thiolate core-shell nanoclusters. J. Am. Chem. Soc 134, 16662–16670 (2012). [PubMed: 22998450]

4. Zheng J et al. Dose Dependencies and Biocompatibility of Renal Clearable Gold Nanoparticles. Angew. Chemie Int. Ed 57, 266–271 (2018).

5. Kwong GA et al. Mass-encoded synthetic biomarkers for multiplexed urinary monitoring of disease. Nat. Biotechnol 31, 63–70 (2013). [PubMed: 23242163]

6. Warren AD et al. Disease Detection by Ultrasensitive Quantification of Microdosed Synthetic Urinary Biomarkers. J. Am. Chem. Soc 136, 13709–13714 (2014). [PubMed: 25198059]

7. Warren AD, Kwong GA, Wood DK, Lin KY & Bhatia SN Point-of-care diagnostics for noncommunicable diseases using synthetic urinary biomarkers and paper microfluidics. Proc. Natl. Acad. Sci. U. S. A 111, 3671–6 (2014). [PubMed: 24567404]

8. Kwon EJ, Dudani JS & Bhatia SN Ultrasensitive tumour-penetrating nanosensors of protease activity. Nat. Biomed. Eng 1, 0054 (2017). [PubMed: 28970963]
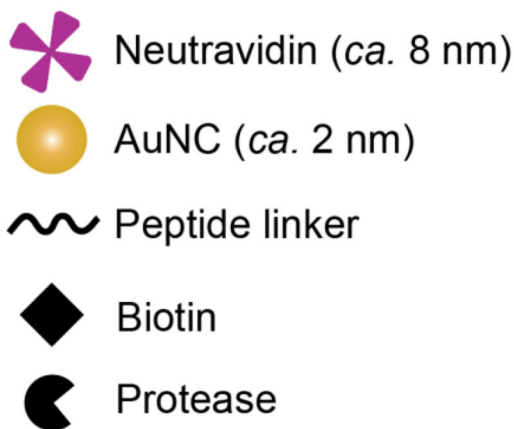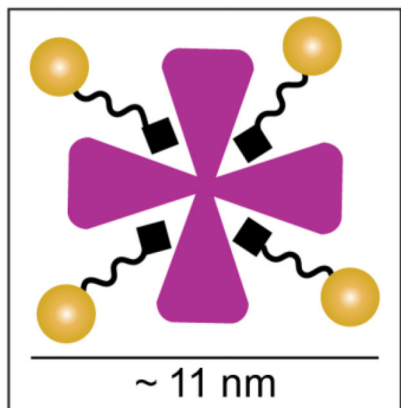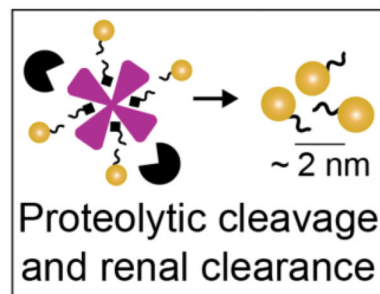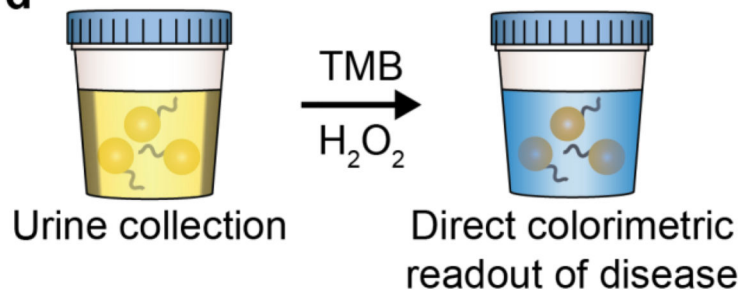
Figure 1. Design of nanocatalyst signal amplification sensing system.
(a) Catalytic gold nanoclusters (AuNCs, *ca.* 2 nm) were conjugated to a neutravidin protein scaffold (*ca.* 8 nm) through a biotinylated protease-cleavable peptide linker. (b) The protease-sensitive nanocluster-neutravidin complex (*ca.* 11 nm) was injected intravenously and designed to specifically disassemble when exposed to the activity of relevant dysregulated proteases at the site of disease. (c) After protease cleavage, liberated *ca.* 2 nm AuNCs were filtered through the kidneys and into urine. (d) AuNCs were detected in cleared urine by measuring their ability to oxidize a chromogenic peroxidase substrate (*e.g.* 3,3′,5,5′-Tetramethylbenzidine, TMB) in the presence of hydrogen peroxide, generating a coloured signal that can be easily read by eye.
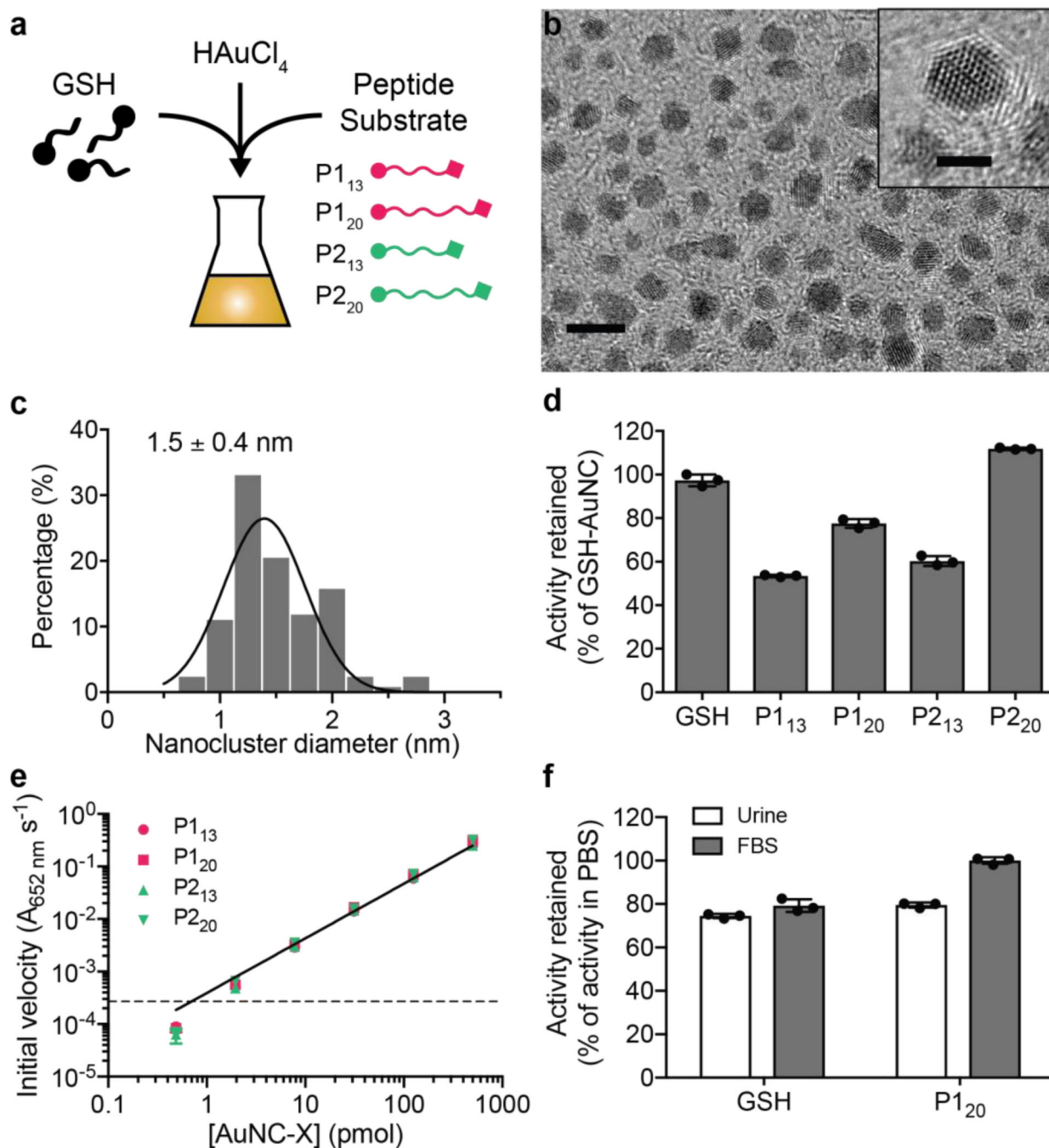
Figure 2. Peptide-functionalized AuNCs exhibit robust catalytic activity.
(a) Schematic showing one-pot synthesis of AuNCs where thiol-terminated
heterobifunctional peptides (P1$_{13}$, P1$_{20}$, P2$_{13}$, P2$_{20}$) were incorporated onto the AuNC
surface. (b) Transmission electron micrograph (TEM) of glutathione-protected AuNCs
(GSH-AuNCs, scale = 5 nm). Inset shows high-resolution TEM of an individual GSH-
AuNC (scale = 2 nm). (c) Histogram showing results of size analysis from TEM images of
GSH-AuNCs (legend shows mean diameter ± s.d., n = 127 particles). Solid line represents
Gaussian fit of size distribution. (d) Catalytic activity of AuNCs capped with different

cysteine containing protease-cleavable peptide linkers (GSH, $P1_{13}$, $P1_{20}$, $P2_{13}$, $P2_{20}$, Table 1; mean ± s.d., $n = 3$ independent experiments). Activity was measured by the absorbance at 652 nm corresponding to the oxidation of the chromogenic peroxidase substrate TMB by H_2O_2 and normalized here to the activity of GSH-AuNCs in PBS. (e) Limit of detection of reporter probes in synthetic urine measured by catalytic activity of AuNCs functionalized with peptides, where $X = P1_{13 \text{ or } 20}$ or $P2_{13 \text{ or } 20}$ (mean ± s.d., $n = 3$ independent experiments). Catalytic activity was measured by initial velocity analysis ($A_{652 \text{ nm}} \text{ s}^{-1}$) of TMB oxidation. Solid line indicates activity for AuNCs is linear over 3 orders of magnitude of particle concentration with nonlinear (log scale) regression least-squares fit, $R^2 = 0.9996$. Dashed line represents limit of detection, which was calculated as 3 standard deviations above the mean background signal. (f) Catalytic activity of GSH-AuNCs and representative AuNC-$P1_{20}$ batch incubated in urine (undiluted) or serum (undiluted FBS) environments for 1 h. Activity was normalized to activity of AuNCs in PBS (mean ± s.d., $n = 3$ independent experiments).
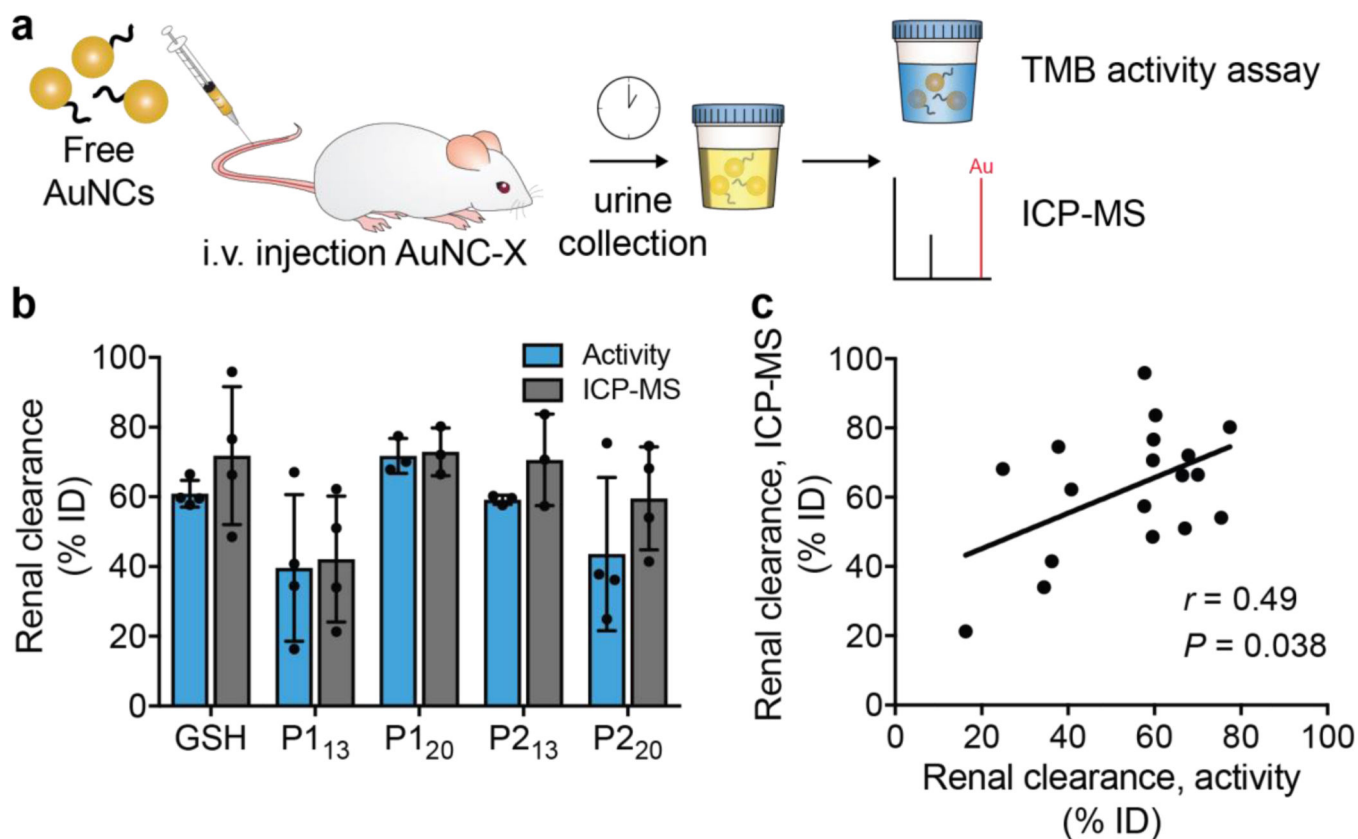
Figure 3. Peptide-functionalized AuNCs clear via the renal system and retain catalytic activity in urine.

(a) Schematic of the renal clearance assay. AuNCs were intravenously (i.v.) injected into Swiss Webster mice, and urine was collected 1 h post-injection. Urine was analysed by both TMB catalytic activity assay and by ICP-MS to measure gold content. (b) Renal clearance efficiency of GSH-AuNC, AuNC-P1$_{13}$, AuNC-P1$_{20}$, AuNC-P2$_{13}$, AuNC-P2$_{20}$ as measured by colorimetric assay (A$_{652\ nm}$) and by ICP-MS (estimated ppb cleared), normalized to activity and gold content, respectively, of the injected dose (mean ± s.d., $n = 3$ or 4 mice per group). (c) Correlation between estimated renal clearance as measured by colorimetric activity assay and by ICP-MS (Pearson's $r = 0.492$ with 95% confidence interval 0.0320 to 0.780, $n = 18$ mice, *$P = 0.0383$).
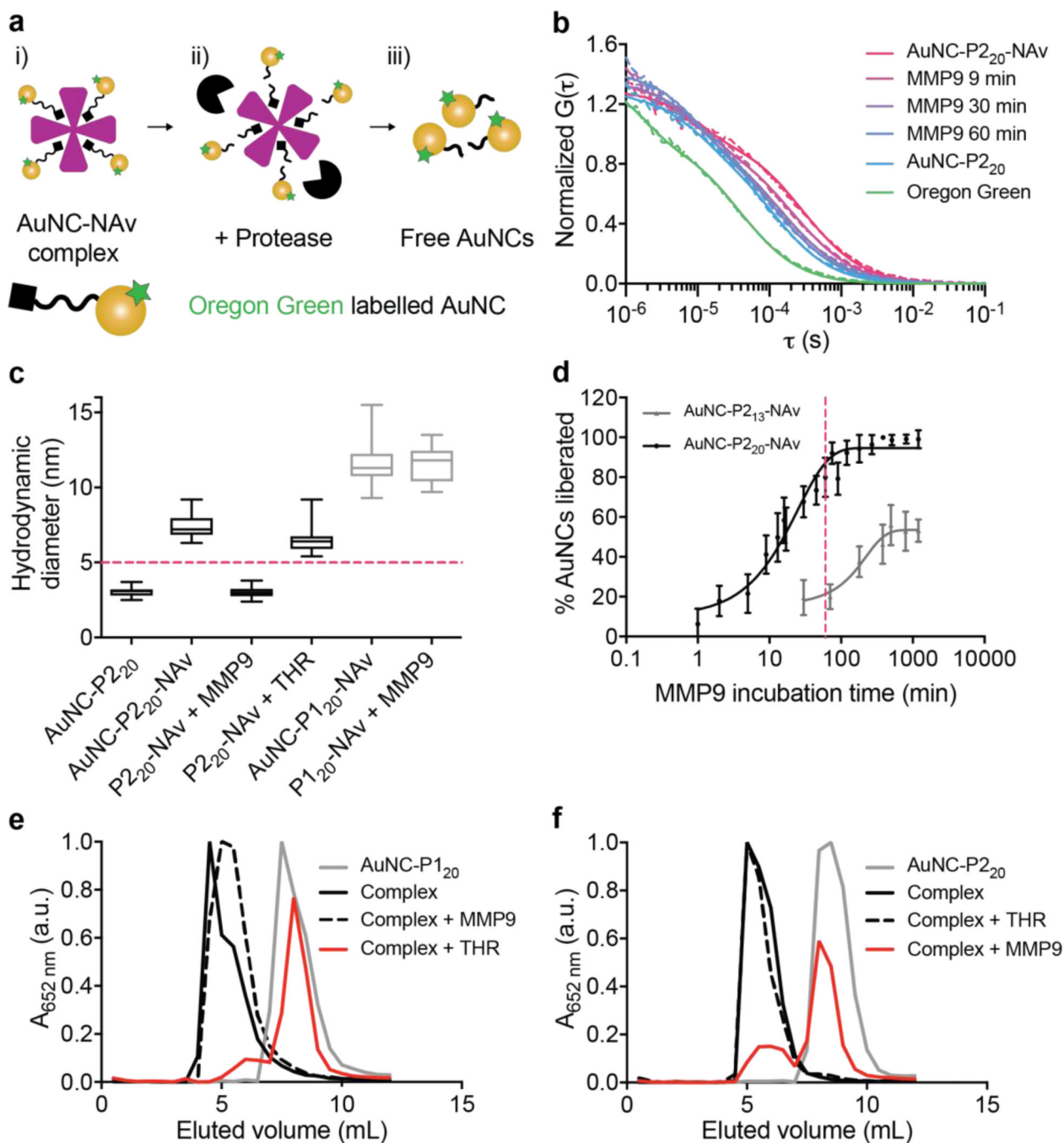
Figure 4. AuNC-neutravidin complexes disassemble *in vitro* in response to protease activity.
(a) Schematic illustration of FCS experiment. (i) AuNCs were labelled with a fluorescent dye and complexed to a neutravidin core. (ii) Dye-labelled AuNC-NAv complexes were incubated with the relevant enzyme: MMP9 or thrombin (THR), (iii) and FCS was used to monitor changes in diffusion time due to enzyme cleavage. (b) Average autocorrelation curves from FCS measurements ($n = 25$ independent measurements) showing AuNC-P2$_{20}$-NAv complex in the presence of MMP9 (50 nM) over time compared to free labelled AuNCs and Oregon Green dye (dashed lines: experimental; solid lines: fits). A clear shift to faster

diffusion times was observed for longer enzyme incubation times (red to blue colour change), indicating cleavage of AuNCs from the complex. (c) Hydrodynamic diameters calculated from FCS autocorrelation curves showing changes in sizes of complexes after enzyme incubation: AuNC-P2$_{20}$-NAv + MMP9 (50 nM, 4.5 h) or thrombin (50 nM, 12 h); AuNC-P1$_{20}$-NAv + MMP9 (50 nM, 12 h). Dashed line represents renal filtration size cut-off of *ca.* 5 nm.[32] Center line represents median, box limits represent upper and lower quartiles, and whiskers represent minimum and maximum values ($n = 25$ independent measurements). (d) Plot of fraction of AuNCs liberated (see FCS in Supplementary Methods) from AuNC-P2$_{13\ or\ 20}$-NAv complex for MMP-responsive complexes composed of either short or long linker incubated with MMP9 (50 nM) up to 16 h (mean ± s.d., $n = 25$ independent measurements). Dashed line at 60 min corresponds to time frame of *in vivo* experiments. (e) Normalized absorbance measuring catalytic activity of gel filtration chromatography (GFC) column fractions associated with AuNC-P1$_{20}$, thrombin-responsive AuNC-P1$_{20}$-NAv complex (Complex), AuNC-P1$_{20}$-NAv (10 μM) incubated with MMP9 (50 nM, 12 h) (Complex + MMP9), and AuNC-P1$_{20}$-NAv complex (10 μM) incubated with thrombin (50 nM, 12 h) (Complex + THR). (f) Normalized absorbance measuring catalytic activity of GFC column fractions associated with AuNC-P2$_{20}$, MMP-responsive AuNC-P2$_{20}$-NAv complex (Complex), AuNC-P2$_{20}$-NAv complex (10 μM) incubated with thrombin (50 nM, 12 h) (Complex + THR), and AuNC-P2$_{20}$-NAv (10 μM) incubated with MMP9 (50 nM, 12 h) (Complex + MMP9). All enzyme incubations were performed at 37 °C and all GFC experiments were repeated independently 3 times with similar results.
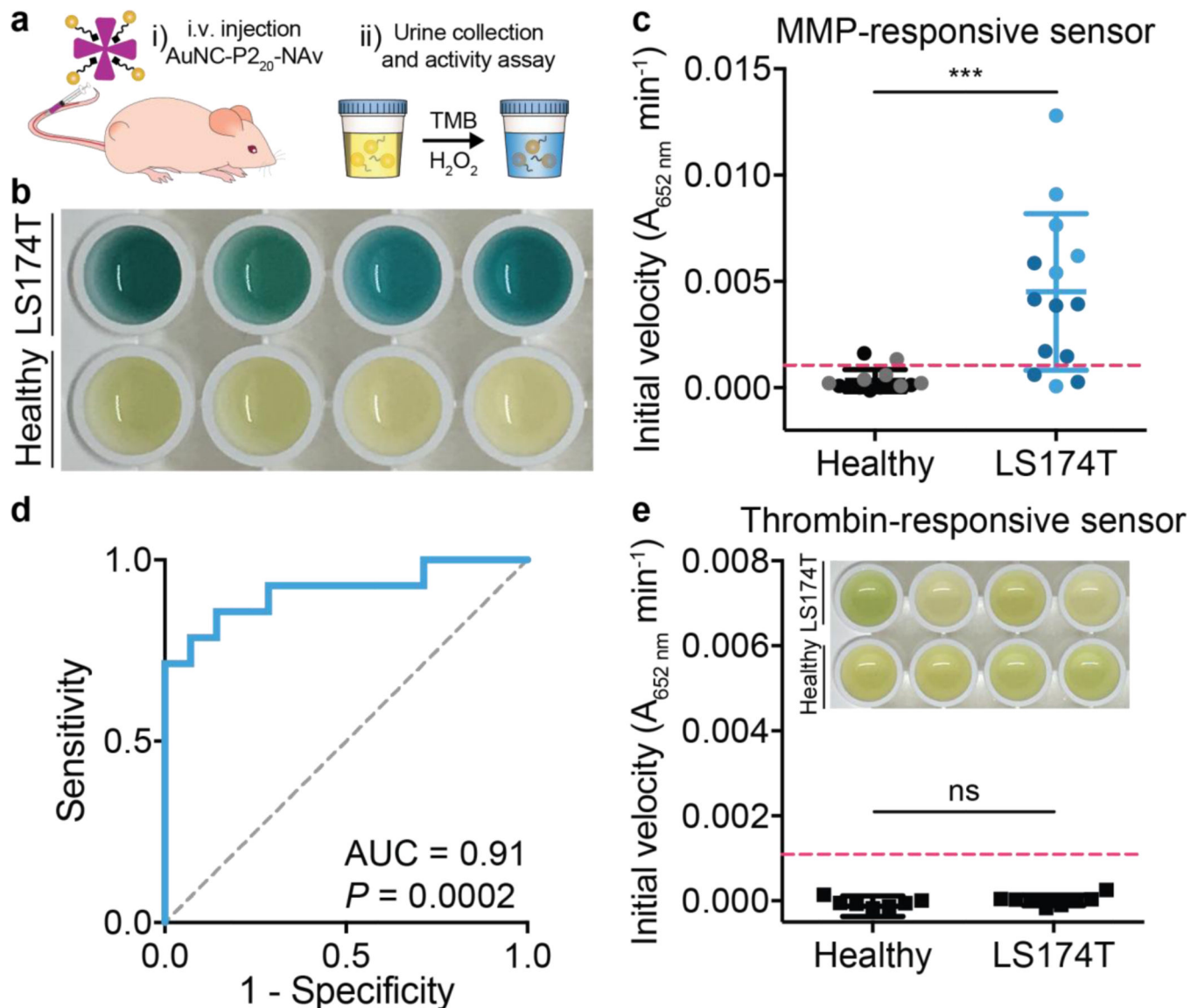
Figure 5. AuNC-functionalized protease nanosensors enable direct colorimetric urinary readout of disease state.

(a) (i) Mice bearing LS174T flank xenografts (2 weeks post inoculation) and age-matched healthy controls were injected intravenously with AuNC-P2$_{20}$-NAv complex. (ii) Urine was collected 1 h p.i., and renal clearance of liberated AuNCs was measured by catalytic activity assay. (b) Photograph of representative examples of colorimetric assay on urine from tumour-bearing (top) and healthy (bottom) mice injected with AuNC-P2$_{20}$-NAv ($n = 4$ mice per group shown). (c) Catalytic activity assay on urine collected from healthy and LS174T tumour-bearing mice 1 h after injection with AuNC-P2$_{20}$-NAv complex (mean $\pm$ s.d., $N = 2$ independent experiments indicated in shades, $n = 6$ (gray and light blue) or 8 (black and dark blue) mice per group, two-tailed Mann-Whitney test, ***$P = 0.0002$). Catalytic activity was measured by initial velocity analysis (A$_{652\ nm}$ min^{-1}), and dashed line represents limit of detection (see Methods). (d) Receiver-operating characteristic (ROC) curve by initial velocity of catalytic activity assay discriminated healthy from diseased mice with an AUC of

0.91 ($N = 2$ independent experiments, $n = 6$ or 8 mice per group as in Fig. 5c, $P = 0.0002$ from random classifier shown in dashed line). (e) Catalytic activity assay on urine from healthy and tumour-bearing mice injected with thrombin-responsive AuNC-P1$_{20}$-NAv complex. Inset: photograph of representative examples. No visible colorimetric development was observed in either group, and there was no statistically significant difference between the two groups (mean $\pm$ s.d., $n = 8$ mice per group, two-tailed Mann-Whitney test, $^{ns}P = 0.161$). Catalytic activity was measured by initial velocity analysis (A$_{652\ nm}$ min^{-1}), and dashed line represents limit of detection (see Methods).

Table 1.

Protease-cleavable thiol-terminated peptide sequences for AuNC synthesis. Catalytic AuNCs were synthesized using GSH and another thiol-terminated protease-cleavable peptide sequence: $P1_{13}$, $P1_{20}$, $P2_{13}$, or $P2_{20}$, where the subscript indicates the number of amino acid residues in each sequence. AuNCs synthesized with the respective peptides are subsequently labelled AuNC-$P1_{13\ or\ 20}$ and AuNC-$P2_{13\ or\ 20}$.

Substrate ($P_{\#aa}$)	Protease specificity	Sequence (↓ represents scissile bond, enzyme recognition motif bolded)	MW (g/mol)	Product (g/mol)
$P1_{13}$	Thrombin	Biotin-SGG**fPR**↓SGGSGGC	1350	846
$P1_{20}$	Thrombin	Biotin-GGGSGGGSGG**fPR**↓SGGGGGC	1750	1275
$P2_{13}$	MMP9	Biotin-GGG**PLG**↓VRGKGGC	1339	683
$P2_{20}$	MMP9	Biotin-GGGGGGGGGG**PLG**↓VRGKGGC	1739	1080